Accelerated Publications

Chlorophyll and Carotenoid Radicals in Photosystem II Studied by Pulsed ENDOR†

Peter Faller,‡ Thorsten Maly,§ A. William Rutherford,‡ and Fraser MacMillan*,§

Institut für Physikalische und Theoretische Chemie, Johann Wolfgang Goethe-Universität, D-60439 Frankfurt am Main, Germany, and Section de Bioénergétique, Département de Biologie Cellulaire et Moléculaire, CNRS URA 2096, CEA Saclay, F-91191 Gif-sur-Yvette, France

Received August 25, 2000; Revised Manuscript Received November 2, 2000

ABSTRACT: The stable carotenoid cation radical ($Car^{\bullet+}$) and chlorophyll cation radical ($Chl_Z^{\bullet+}$) in photosystem II (PS II) have been studied by pulsed electron nuclear double resonance (ENDOR) spectroscopy. The spectra were essentially the same for oxygen-evolving PS II and Mn-depleted PS II. The radicals were generated by illumination given at low temperatures, and the ENDOR spectra were attributed to $Car^{\bullet+}$ and $Chl_Z^{\bullet+}$ on the basis of their characteristic behavior with temperature as demonstrated earlier [Hanley et al. (1999) *Biochemistry 38*, 8189−8195]: i.e., (a) the $Car^{\bullet+}$ alone was generated by illumination at ≤20 K, while $Chl_Z^{\bullet+}$ alone was generated at 200 K, and (b) warming of the sample containing the $Car^{\bullet+}$ to 200 K resulted in the loss of the signal attributable to $Car^{\bullet+}$ and its replacement by a spectrum attributable to the $Chl_Z^{\bullet+}$. A map of the hyperfine structure of $Car^{\bullet+}$ in PS II and in organic solvent was obtained. The largest observed hyperfine splitting for $Car^{\bullet+}$ in either environment was in the order of 8−9 MHz. Thus, the spin density on the cation is proposed to be delocalized over the carotenoid molecule. The pulsed ENDOR spectrum of $Chl_Z^{\bullet+}$ was compared to that obtained from a Chl *a* cation in frozen organic solvent. The hyperfine coupling constants attributed to the β-protons at position 17 and 18 are well resolved from $Chl_Z^{\bullet+}$ in PS II (10.8 and 14.9 MHz) but not in Chl $a^{\bullet+}$ in organic solvent (12.5 MHz). This suggests a more defined conformation of ring IV with respect to the rest of the tetrapyrrole ring plane of $Chl_Z^{\bullet+}$ than Chl $a^{\bullet+}$ probably induced by the protein matrix.

Photosystem II (PS II)[1] catalyzes the light-driven water oxidation resulting in oxygen evolution. Absorption of a photon leads to a charge separation between a chlorophyll species, P_{680}, and a pheophytin molecule. The pheophytin anion transfers the electron to a quinone, Q_A, whereas the P_{680} cation is reduced by a tyrosine (Tyr_Z), which is reduced in turn by abstracting an electron from the Mn cluster. The latter acts as an accumulator of positive charge equivalents and is thought to be the site for water oxidation (for reviews of PS II see refs *1* and *2*).

There are several conditions known, some of them of physiological relevance, in which the donation of Tyr_Z to P_{680}^+ is inhibited or retarded, allowing the highly oxidizing P_{680}^+ ($E_M \sim 1.1$ V) to abstract an electron from other sources. Chlorophyll (Chl_Z), cytochrome b_{559}, and a carotenoid have been identified as electron donors to P_{680}^+ under various conditions (*3*−*6*). An electron-transfer pathway involving cyt b_{559} and Chl_Z has been suggested to protect the PS II against uncontrolled oxidative reactions of the very oxidizing P_{680}^+ (for a review see ref *7*). Recently, evidence has been obtained for the involvement of carotenoid in this pathway (*8*), most likely one of the all-trans β-carotenes in the reaction center. It was shown that the carotenoid radical ($Car^{\bullet+}$) can be stoichiometrically generated by illumination of PS II at 20 K, and furthermore, by warming to 120−200 K, an electron transfer from Chl_Z takes place, resulting in reduced carotenoid and $Chl_Z^{\bullet+}$. These results suggested the following electron pathway: $Chl_Z \rightarrow Car \rightarrow P_{680}$ (*8*). In addition, several spectroscopic studies of $Car^{\bullet+}$ have been performed (*8*−*12*).

It is possible to characterize these radicals using low-temperature electron paramagnetic resonance (EPR) spec-

† Research supported by a Deutsche Forschungsgemeinschaft grant (DFG-Sfb472/P15 to F.M.), a European Union TMR Research Network grant (FMRX-CT98-0214 to A.W.R.), a travel grant from the ESF program: Biophysics of Photosynthesis (to P.F.), the CEA Saclay, and a grant from the Swiss National Science Foundation (to P.F.).

* Corresponding author. Fax: (+49) 69 798 29 404. E-mail: fm@masklin.anorg.chemie.uni-frankfurt.de.

‡ Département de Biologie Cellulaire et Moléculaire, CNRS URA 2096.

§ Johann Wolfgang Goethe-Universität.

[1] Abbreviations: Car, redox-active carotenoid; Chl, chlorophyll; Chl_z, redox-active chlorophyll in PS II; E_m, midpoint potential at pH 7; EDTA, ethylenediaminetetraacetic acid; EPR, electron paramagnetic resonance; ENDOR, electron nuclear double resonance; hfc, hyperfine coupling constant; ΔH_{pp}, the EPR line width defined as the peak to peak width of the first derivative signal; MES, 2-(*N*-morpholino)-ethanesulfonic acid; PS II, photosystem II; Q_A, the first protein-bound plastoquinone acting as an electron acceptor; Q_B, the second protein-bound plastoquinone acting as an electron acceptor; $Q_A^{-\bullet}$-Fe^{2+}, the $Q_A^{-\bullet}$ state magnetically coupled with the high-spin, non-heme ferrous ion; P_{680}, the chlorophyll species that is the primary electron donor in PS II; $Tyr_Z^{\bullet}$, redox-active tyrosine 161 of D1 protein which acts as a kinetically competent electron carrier; $Tyr_D^{\bullet}$, redox-active tyrosine 160 of D2 protein which forms a stable tyrosyl radical.

10.1021/bi002029l CCC: $20.00
Published on Web 12/16/2000

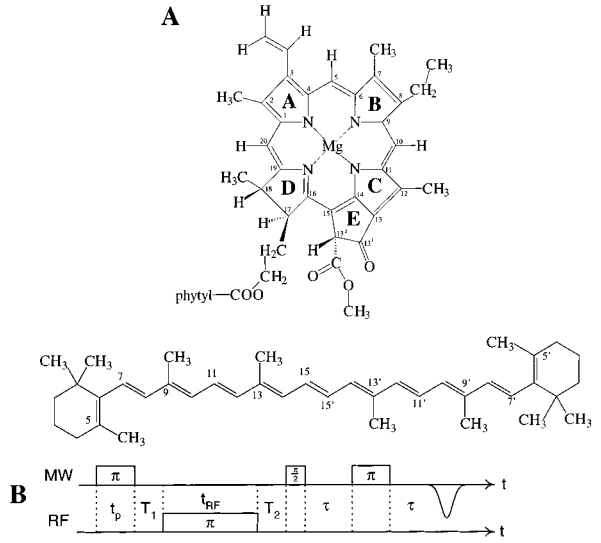

FIGURE 1: (A) Molecular structure of chlorophyll *a* with numbering and of *β*-carotene with numbering. (B) Davies ENDOR pulse sequence.

troscopy. However, at X-band frequencies (9 GHz) the resulting spectra are unresolved. EPR signals from $Car^{\bullet+}$ and $Chl_Z^{\bullet+}$ appear quite similar, having a broad unresolved line shape of approximately 10 G and an average *g*-value close to the free electron value of 2.0023. Several methods exist to characterize and differentiate such species. High-field EPR can be used to resolve the respective *g*-tensors; however, it has been shown for carotenoid model systems (*13*), for $Car^{\bullet+}$ in PS II (*14*), and for a Chl cation radical in PS II (*15*) that very high fields are required (>10 T) and that even then not all components of the *g*-tensor are clearly resolved. Another method for looking at the interaction of weakly coupled magnetic nuclei or magnetic nuclei with a small gyromagnetic ratio (γ_N) is electron spin−echo envelope modulation (ESEEM) spectroscopy. This pulsed EPR technique has been successfully applied to such radicals in the past. The hyperfine parameters of Chl *a* cations have been studied in depth (e.g., ref *16*), and recently the first observation of the interaction of the $Car^{\bullet+}$ in PS II with nitrogen atoms of its surrounding protein was reported (*11*). For a detailed investigation of the spin density distribution within the radical itself, the method of electron nuclear double resonance (ENDOR) spectroscopy can be applied (for an introduction see refs *17* and *18*). This method resolves hyperfine (hf) interactions between the electron spin and the nuclear spins of surrounding magnetic nuclei. A map of the hyperfine structure of the radical in question and thus its spin density distribution is then obtained. There exists an extensive literature on cw ENDOR spectroscopy of carotenoid radicals (*19*−*23*). It has been determined, in combination with MO calculations (*19*, *20*) from these model systems that the spin density is delocalized over the whole length of the polyene chain.

There is also considerable hyperfine information in the literature on Chl *a* cation radicals (e.g., refs *24*−*31*). Nearly all of these experiments have been performed using cw ENDOR methods. Huber et al. (*27*) observed that the temperature dependence of these hyperfine interactions is quite different for different nuclei within the radical. The protons at positions 17 and 18 (see Figure 1A) are very difficult to detect at low temperatures using cw ENDOR experiments. A combination of ENDOR and MO calculations (RHF-INDO/SP) have demonstrated that for bacteriochlorophyll (BChl) *a* cations these hyperfine interactions are however quite sensitive to the geometry and puckering of ring IV (see Figure 1A; *30*). It is expected that this holds also for Chl *a* cations. It is known that distorting the porphyrin ring destabilizes the HOMO, causing such molecules to become easier to oxidize (*32*, *33*).

It has been recently shown (*8*) that it is possible to generate a pure $Car^{\bullet+}$ state in near stoichiometric amounts in PS II with the virtual absence of $Chl_Z^{\bullet+}$. In principle, this should allow the study of $Car^{\bullet+}$ using pulsed ENDOR spectroscopy. The specific temperature dependence of electron transfer from Chl_Z to $Car^{\bullet+}$ upon raising the temperature to higher than 120 K allows the two radicals to be identified and studied separately. Here we apply the method of pulsed ENDOR spectroscopy to characterize the $Car^{\bullet+}$ and $Chl_Z^{\bullet+}$ cations in PS II.

MATERIALS AND METHODS

Photosystem II Samples. PS II membranes from spinach chloroplasts were prepared according to Berthold et al. (*34*) with the modifications described in Ford and Evans (*35*) and were stored at 77 K until used. Mn was depleted from PS II by incubating the membranes (1 mg of Chl /mL) in the presence of a freshly made solution of NH_2OH (2 mM) at 0 °C for 15 min in room light. The sample was then transferred into complete darkness, where the NH_2OH concentration was increased to 4 mM and incubated again for 30 min at 0 °C. The membranes were then precipitated by centrifugation and washed five times in a buffer containing $MgCl_2$ (5 mM), NaCl (10 mM), EDTA (1 mM), and MES (50 mM, pH 6.3), by successive resuspension and centrifugation steps in order to remove NH_2OH. The final pellet was dissolved in NaCl (15 mM), sucrose (0.3 M), and MES (50 mM, pH 6.5). All of the washing steps described above were performed in total darkness. In such PS II membranes the Tyr_D is almost totally reduced as can be concluded from the absence of the EPR signal known to originate from Tyr_D. The number of spins per PS II for $Chl^{\bullet+}/Car^{\bullet+}$ was assessed relative to the Tyr_D signal obtained in a similar sample by comparison of the echo intensities.

Sample Preparation. ENDOR spectroscopy was performed on PS II samples containing about 6 mg of Chl/mL in 4 mm outer diameter EPR tubes, which were filled in total darkness and frozen at 77 K. Illumination at 5 K was done directly in the cavity using a 100 W tungsten lamp filtered through 5 cm of water. Typical illumination times were between 15 and 30 min. This is due to the limited light access in the Bruker dielectric ring ENDOR cavity. During the illumination the sample was rotated several times.

Preparation of in Vitro Chl a and Car Radicals. For the oxidation of Chl *a*, a solution of Chl *a* (1 mM) in a mixture of methylene chloride (CH_2Cl_2) and tetrahydrofuran (THF) (10:1) was bubbled for several minutes with argon. A 10-fold molar excess of I_2 in CH_2Cl_2 in the presence of an equimolar amount of $AgClO_4$ in acetonitrile (AcCN) was then added, after which the solution was rapidly frozen in liquid nitrogen. All procedures were performed in dim light.

For the carotenoid sample a solution of *β*-carotene (10 mM) in a mixture of CH_2Cl_2 and THF (10:1) was also

bubbled with argon for several minutes. Again the solution was then treated with a 10-fold molar excess of I_2 in CH_2Cl_2 in the presence of an equimolar amount of $AgClO_4$ in acetonitrile (AcCN). The sample was then rapidly frozen in liquid nitrogen. All solvents had been previously degassed several times under high vacuum.

Instrumentation. X-Band EPR spectra were measured on a Bruker E-580 spectrometer using a Bruker EPR cavity (MD5-W1) equipped with an Oxford helium flow cryostat (CF935). The field-swept spectrum was obtained by recording the amplitude of the echo as a function of the magnetic field after a two-pulse sequence ($\pi/2-\tau-\pi/2$). Pulsed ENDOR spectra were recorded on a Bruker E-580 spectrometer equipped with a Bruker E-560D pulsed ENDOR accessory, a Bruker MD5EN-W1 pulsed ENDOR probe head, a 2 kW Dressler solid-state radio frequency amplifier (LPPA 10020 LF), and an Oxford helium cryostat (CF 935). In a Davies ENDOR ($\pi-T_1-$RF pulse $T_2-\pi/2-\tau-\pi-\tau-$echo) (Figure 1C) experiment (*36*), a selective microwave π pulse (t_p) first inverts polarization of an electron spin transition. An RF π pulse (t_{RF}) is then applied to the appropriate nuclear transition to induce sublevel polarization transfer. The final electron spin polarization is monitored by the spin−echo intensity generated in a subsequent two-pulse detection sequence. Davies ENDOR spectra were recorded as the RF-induced change in echo surface while the RF frequency was swept. The value of t_p was set to optimize the echo inversion and the one of t_{RF} to maximize the ENDOR effect. A 2−5 μs delay was included between the RF pulse and the two-pulse detection sequence to avoid interference from RF ringdown during the two-pulse detection sequence.

ENDOR in Frozen (Disordered) Solutions. In frozen solutions anisotropic g and hyperfine (hf) interactions are no longer averaged out, and contributions from all molecular orientations relative to the magnetic field contribute to the EPR spectrum, which is therefore significantly broadened due to the g- and hf-tensor anisotropy. For the NMR (ENDOR) transition frequencies in carotenoid radicals the contributions of the relatively small g-tensor anisotropy can be neglected at X-band. The first-order NMR (ENDOR) frequencies in this case are given for each proton by (*37*)

$$\nu_{\pm}^2(\text{ENDOR}) = \nu_H^2 + {}^1/_4(lAAl) \pm \nu_H(lAl) \qquad (1)$$

where l is the unit vector along the field B_0, with components $l_{x,y,z}$, the direction cosines of B_0 in the reference axis system. The two frequencies ν_+ and ν_- are in general no longer symmetric about ν_H for all orientations. However, when B_0 is along one of the principal axes (x,y,z) of A, eq 1 reduces to

$$\nu_{\pm}^2(\text{ENDOR}) = |\nu_H \pm A_{ii}| \qquad (2)$$

($i = x,y,z$), and the respective hf tensor principal component is obtained directly from the separation of ν_+ and ν_-. In the center of the X-band (9.5 GHz) EPR spectrum all orientations of the molecules with respect to B_0 contribute to the EPR intensity. Therefore, the corresponding ENDOR spectrum exhibits a typical powder pattern. This is obtained by summation over all possible orientations of l in eq 1. From the turning points of the spectra the principal values of the hf tensors can be directly obtained. For axially symmetric hf tensors with small anisotropy (e.g., methyl group protons) usually both principal values $A_{||}$ and $A_{\perp}$ can easily be obtained. The spectra have been analyzed by spectral simulation using the program from Rohrer et al. (*38*).

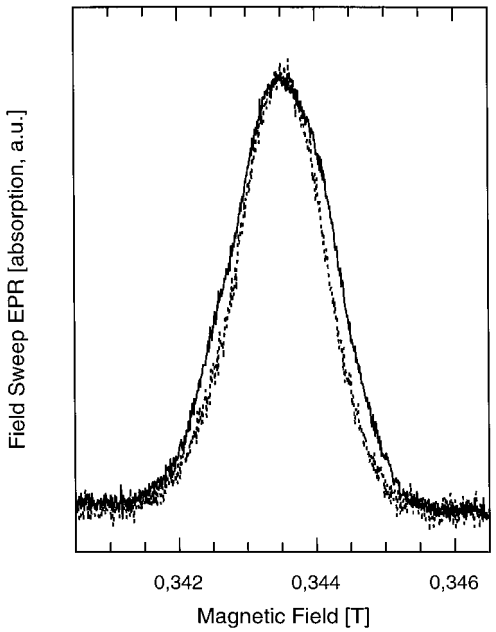

FIGURE 2: (A) 9 GHz field-swept EPR spectrum of the radicals generated by low-temperature illumination. Dark-adapted samples were illuminated at 5 K (dotted line) and 200 K (solid line); for details see Materials and Methods. Experimental conditions: t_p, 48 ns; τ, 280 ns; shot repetition time, 200 ms; 4 scans; $T = 20$ K.

RESULTS

No significant difference between the ENDOR spectra of either chromophore, $Car^{\bullet+}$ and $Chl_Z^{\bullet+}$, in untreated or Mn-depleted PS II preparations was observed. Thus, only the Mn-depleted PS II spectra are shown.

Figure 2 shows the effects of 5 K (dotted line) and 200 K (solid line) illumination of Mn-depleted PS II enriched membranes. Neither of the field-swept EPR spectra contain the stable tyrosyl radical, $Tyr_D^{\bullet}$. This species is absent due to reduction by hydroxylamine (see Materials and Methods). In both samples the light-induced radicals are centered at $g \sim 2.0026$, are about 9.0−10.0 G wide, and amount to a yield of approximately 60−80% per PS II based on a comparison with the dark stable Tyr_D (see Materials and Methods). Only a very slight difference in line width is observed, with the sample illuminated at 200 K having a slightly larger line width.

Figure 3 shows the pulsed ^{1}H ENDOR spectrum of the sample illuminated at 5 K, conditions which lead to the formation of the Car cation (A). Also shown in Figure 3 is the spectrum obtained from β-carotene oxidized by iodine in frozen dichloromethane (B). In frozen solutions protons from methyl groups give rise to narrow and intense ENDOR lines (*39*). As has been previously demonstrated, methyl hyperfine couplings (hfc's) in carotene radicals have very little anisotropy while lines from α-protons are often broadened and not easily detected. From a simulation of the spectra in Figure 3, several line pairs spaced symmetrically around the free proton Larmor frequency can be determined

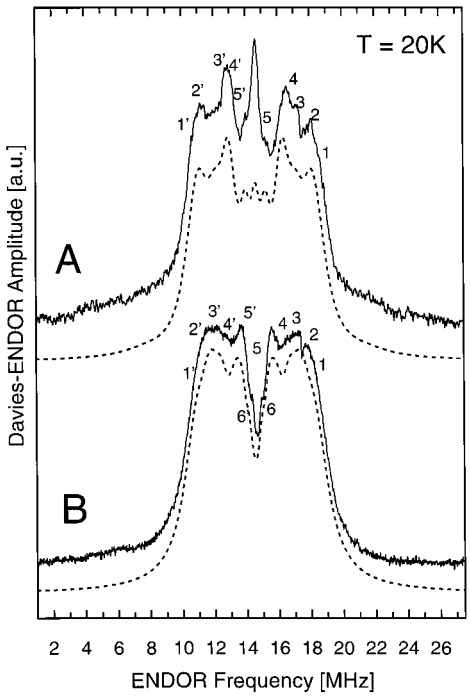

FIGURE 3: (A) Davies ENDOR spectrum of the PS II sample illuminated at 5 K and measured at 20 K (solid line) and its simulation (dotted line). (B) Davies ENDOR spectrum (solid line) of I_2-oxidized Car$^{\bullet+}$ in CH_2Cl_2 recorded at 20 K and its simulation (dotted line). The line pairs belonging to proton hyperfine couplings (hfc's) are labeled (1, 1′, etc.) and are listed in Table 1. Experimental conditions: t_p, 200 ns; τ, 500 ns; t_{RF}, 8 μs (~500 W); shot repetition time, 200 ms (A) and 8 ms (B); number of scans, 310 (A) and 717 (B).

(*38*) and are listed in Table 1. It is clear that the hfc's obtained for Car$^{\bullet+}$ in PS II and for Car$^{\bullet+}$ in vitro are quite similar. β-Carotene has six methyl groups but only in three distinct positions (see Figure 1). There was no indication that the protein matrix of PS II induces a loss of this symmetry. Therefore, the Car$^{\bullet+}$ spectrum in PS II was simulated using only three distinct types of methyl tensors. It is apparent that the largest hf splitting observed in either sample is of the order of ~8 MHz, which would suggest a spin distribution which is delocalized (see Discussion). This is of interest, since a localization of the hole on Car$^{\bullet+}$ has been considered, when discussing the resonance Raman studies of Car$^{\bullet+}$ in D_1/D_2 preparations (*10*). There is no indication of any ^{14}N hfc's.

Figure 4A shows the pulsed ^{1}H ENDOR spectrum of the PS II sample illuminated at 200 K, conditions that lead to the formation of $Chl_Z^{\bullet+}$. Also shown as spectrum B is the sample which was illuminated at 5 K and then dark-adapted in the ENDOR cavity at 200 K for 30 min. As is clearly seen, both signals are almost identical and quite different from those observed in Figure 3, which are assigned to the Car$^{\bullet+}$ species. The main differences are the presence of ^{14}N hfc's at low frequencies and in the center of the spectrum, where the relative intensity assigned to the matrix proteins is much larger for $Chl_Z^{\bullet+}$ than Car$^{\bullet+}$. The known conversion from Car$^{\bullet+}$ to $Chl_Z^{\bullet+}$ upon incubation at 200 K corroborates the assignment of the spectra in Figures 3 and 4 to Car$^{\bullet+}$ and $Chl_Z^{\bullet+}$, respectively (*8*).

Figure 4C shows the Chl $a^{\bullet+}$, generated by oxidation of Chl *a* with iodine in CH_2Cl_2/THF in the presence of $AgClO_4$. The hfc's deduced from the spectra by simulation are given in Table 2. They agree very well with previous data from the literature (Table 2). The hfc's assigned to the methyl protons at positions 2, 7, and 12 are almost identical to hfc's measured in this work. The smaller coupling pair (5,5′−6,6′; see Figure 4) results from two methyl groups while the larger coupling pair (2,2′−3,3′−4,4′; see Figure 4) arises from one, as has been clearly shown from solution ENDOR studies of the Chl $a^{\bullet+}$ (*28*) as well as from their temperature dependence (*31*). The Chl $a^{\bullet+}$ generated in PS II appears more complex; however, spectral simulations using similar values for the hfc's from the methyl groups allow a putative assignment (Table 2). In contrast to the in vitro Chl $a^{\bullet+}$, where the hfc's of the methyl groups at positions 2 and 7 are not resolved, the simulation of $Chl_Z^{\bullet+}$ in PS II resolved three distinct coupling pairs, assigned to the three hfc's of the methyl groups 2, 7, and 12.

Apart from the prominent features arising from the hfc of the methyl protons, additional features are also observed. There are low-field resonances (at 4−6 MHz) that have no symmetrical partner around the proton Larmor frequency. These are assigned in analogy to Figure 3 in Jegerschöld et al. (*41*) to ^{14}N hyperfine interactions. The magnitude of these couplings is similar to those observed for model Chl $a^{\bullet+}$ radicals (*42*) but is not further investigated here.

A broad feature with an hfc of about 12.5 MHz in the in vitro Chl $a^{\bullet+}$ spectrum was previously assigned to the β-protons at positions 17 and 18 (*24*). In contrast, the spectrum of $Chl_Z^{\bullet+}$ in PS II exhibits two hfc's at 14.9 and 10.8 MHz, indicating that the hfc's for the protons at positions 17 and 18 are resolved in PS II. Due to relaxation effects and also due to the fact that these protons can take up a broad distribution of orientations relative to the ring, it has been previously shown that these hfc's are difficult to detect in in vitro Chl $a^{\bullet+}$ at low temperatures (*27*, *28*). This appears not to be the case for the $Chl_Z^{\bullet+}$ in PS II, which might suggest a more locked (or defined) conformation of Chl_Z. However, the previous experiments on in vitro Chl $a^{\bullet+}$ were all performed in the cw mode. Until now, there is only one report of a pulsed ENDOR experiment on in vitro BChl *a* cations (*43*) which also reveals the presence of a broad feature assigned to a distribution of orientations for the β-H's at positions 17 and 18.

It is clear that these assignments demonstrate that the signal obtained by 200 K illumination of PS II or by annealing after 5 K illumination is the same species and that it can be assigned to a monomeric Chl *a* cation ($Chl_Z^{\bullet+}$). The assignments of the hyperfine couplings to both Car$^{\bullet+}$ and $Chl_Z^{\bullet+}$ have been checked by EPR simulations and agree very well with the observed experimental EPR line widths.

DISCUSSION

The present data demonstrate the ability of ^{1}H ENDOR spectroscopy to differentiate between electron donors in PS II. The X-band EPR signals arising from Car and Chl cations are almost indistinguishable (*8*), and indeed the carotenoid has remained misassigned for more than 15 years. We have used the illumination and temperature regime defined by Hanley et al. (*8*) to obtain the two radicals independently and have resolved their ^{1}H ENDOR spectra. The identities of the radicals are confirmed through the determination of

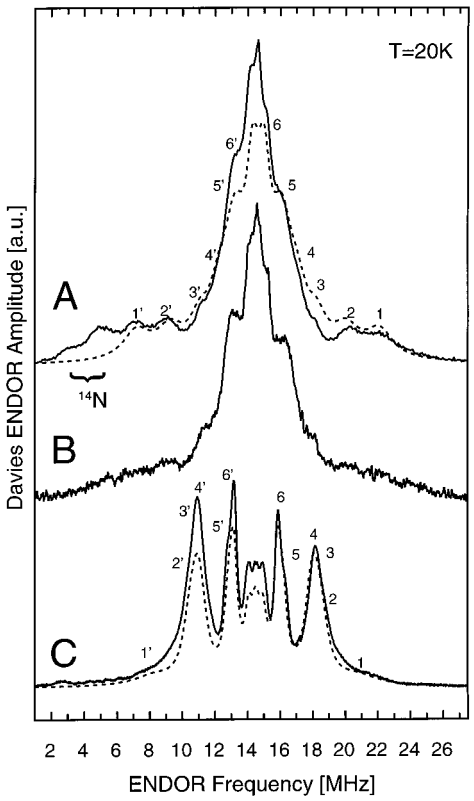

FIGURE 4: Davies ENDOR spectra of (A) PS II illuminated at 200 K and measured at 20 K (solid line) and its simulation (dotted line). (B) Spectrum of PS II illuminated at 5 K and subsequently incubated at 200 K for 30 min and measured at 20 K. (C) Chl $a^{\bullet+}$ in CH_2Cl_2/THF (generated by oxidation with I_2) (solid line) and its simulation (dotted line). The line pairs belonging to certain proton hyperfine couplings (hfc's) are labeled (1, 1′, etc.) and are listed in Table 2. The range in which lines associated with ^{14}N nuclei occur is indicated in the spectrum but is not analyzed here. Experimental conditions: t_p, 200 ns; τ, 500 ns; t_{RF}, 9 μs (∼500 W); shot repetition time, 200 ms (A and B) and 100 ms (C); number of scans, 400 (A), 221 (B), and 458 (C).

their ^{1}H hfc's and, in particular, the ^{14}N hfc's and ^{1}H's at positions 17 and 18 for the $Chl_Z^{\bullet+}$. The ENDOR study performed here provides a more complete study of the electronic structure of these species and is indeed the first observation by ENDOR spectroscopy of a carotenoid cation radical in a protein.

Table 2: Methyl Proton Hyperfine Tensor Components (in MHz) of $Chl_Z^{\bullet+}$ and Chl $a^{\bullet+}$ in Vitro

		$Chl_Z^{\bullet+}$			Chl $a^{\bullet+}$		
molecular position[a]	tensor component	label[b]	this work[c]	ref[d]	label	this work[c]	ref[e]
12	A_{11}	4,4′	6.8	7.3	4,4′	6.45	6.45
	A_{22}	4,4′	6.8	7.3	2,2′	8.5	7.35
	A_{33}	3,3′	8.0	8.2	3,3′	7.0	8.55
	A_{iso}		7.2	7.6	7,6	7.32	7.45
7	A_{11}	6,6′	4.5	3.4	6,6′	2.6	2.75
	A_{22}	6,6′	4.5	3.4	5,5′	3.8	2.75
	A_{33}	5,5′	5.7	4.1	6,6′	2.6	3.90
	A_{iso}		4.9	3.6		3.0	3.0
2	A_{11}	7,7′	2.5		6,6′	2.5	
	A_{22}	6,6′	3.8	nd	5,5′	3.7	nd
	A_{33}	7,7′	2.5		6,6′	2.5	
	A_{iso}		2.9	2.8		2.9	3.0
17	A_{iso}	2,2′	10.8	10.8	1,1′	12.5	10.2
18	A_{iso}	1,1′	14.9				

[a] See Figure 1 for positions. [b] See Figure 4 for labels. [c] Taken from ENDOR simulations (*38*), error ± 100 kHz except positions 17 and 18, ±500 kHz; nd, not determined. [d] From ref *40*. [e] From ref *31*.

The magnitude of the observed hyperfine couplings is quite similar to those seen in model carotene cations studied here. The hfc's determined by simulation of the pulsed ENDOR spectra of $Car^{\bullet+}$ in PS II and in vitro exhibit differences from those hfc's determined previously from in vitro $Car^{\bullet+}$ (see Table 1). The most striking difference is the absence of a 13−15 MHz coupling which has previously been observed and also calculated by RHF-INDO/SP methods (*19*, *20*). cw ENDOR measurements, however, of a carotene cation radical on silica−alumina solid supports were also lacking this 13−15 MHz coupling (*21*). This was ascribed to different (slower) rotational motion of the C_{13} (see Figure 1) methyl group, resulting in line broadening and therefore escaped detection. Recent density functional theory (DFT) calculations (Dr. Fahmi Himo, Stockholm University, personal communication) suggest that the spin density is delocalized

Table 1: ^{1}H Hyperfine Tensor Components (in MHz) of $Car^{\bullet+}$ in PS II and in Vitro

		$Car^{\bullet+}$/PS II			$Car^{\bullet+}$ in vitro			
molecular position[a]	tensor component	label[b]	this work[c]	DFT[d]	label[b]	this work[c]	ref[e]	INDO[f]
13,13′	A_{11}	3,3′	5.5		5,5′	2.6	15.9	
	A_{22}	3,3′	5.0		4,4′	3.8	15.9	
	A_{33}	4,4′	4.5		5,5′	2.6	17.0	
	A_{iso}		5.0	5.2		3.0	16.2	12.2/12.5
9,9′	A_{11}	2,2′	7.2		3,3′	6.45	8.8	
	A_{22}	2,2′	7.2		1,1′	8.5	8.8	
	A_{33}	2,2′	7.2		2,2′	7.0	9.2	
	A_{iso}		7.2	8.4		7.32	8.9	8.1/8.5
5,5′	A_{11}	5,5′	3.3		5,5′	2.5	2.5	
	A_{22}	5,5′	3.3		4,4′	3.7	2.5	
	A_{33}	5,5′	3.3		5,5′	2.5	2.8	
	A_{iso}		3.3	5.4		2.9	2.6	2.2/2.3
15 (α-H)	A_1	1,1′	3.5/7.0/9.0	3.4/5.0	6,6′	1.5−3.0		

[a] See Figure 1 for positions. [b] See Figure 3 for labels. [c] ENDOR simulations (*38*), error ± 100 kHz. [d] Gaussian-94, B3LYP(6-31G(d,p))//B3LYP/3-21G (F. Himo et al., unpublished). [e] From ref *19*. [f] From ref *20*.

over the whole π-conjugated system which also includes part of the two headgroups resulting in hfc's < 8−9 MHz. This is in disagreement with previous INDO-type calculations (*19*, *20*). More studies are needed to resolve the exact reason for these observed differences. The $Car^{\bullet+}$ formed in PS II might be a useful system for this, because it can be selectively generated and is expected to be well isolated by the protein matrix from other $Car^{\bullet+}$ and from negative charges. Such studies are currently in progress (F. Himo, T. Maly, T. F. Prisner, and F. MacMillan, unpublished).

^{1}H hfc's of methyl groups give rise to the intense ENDOR lines observed here in frozen solution. Chl *a* contains three such methyl groups while Car has six, but only in three distinct positions for the isolated molecule (see Figure 1). By comparison of the hfc's of $Car^{\bullet+}$ and $Chl_Z^{\bullet+}$ in PS II, it turns out that their values are quite similar (see Tables 1 and 2). Nevertheless, the overall shape of the spectra is very different, because the intensities and anisotropies of the lines attributed to the three methyl groups 2, 7, and 12 in $Chl_Z^{\bullet+}$ are different from the methyl groups 5/5′, 9/9′, and 13/13′ in $Car^{\bullet+}$. The intense matrix peak in the $Chl_Z^{\bullet+}$ spectrum also suggests a different environment to that seen for $Car^{\bullet+}$ and/or a more localized spin density distribution. Another prominent difference between the $Car^{\bullet+}$ and $Chl_Z^{\bullet+}$ ENDOR is the larger hfc's which are assigned to the protons at positions 17 and 18 in Chl_Z and the ^{14}N hf interactions that are not detected in the $Car^{\bullet+}$ ENDOR spectrum. Although ESEEM spectroscopy has observed the coupling from a ^{14}N nucleus to $Car^{\bullet+}$ (*11*), this has as yet not been observed in the ENDOR spectrum. Depending on the magnitude and anisotropy of such an interaction, ENDOR spectroscopy may be less sensitive to such interactions.

It is of interest to compare the present results with relevant data in the literature. Rigby et al. (*40*), MacMillan et al. (*44*), and Jegerschöld et al. (*41*) have all investigated PS II membrane fragments using cw ENDOR spectroscopy under comparable conditions but where PS II was illuminated at different temperatures (77, 123, and 200 K, respectively). It seems clear from the work of Hanley et al. (*8*) that these spectra indeed all arise from $Chl_Z^{\bullet+}$ although some contamination from residual $Car^{\bullet+}$ may be present in the sample illuminated at 77 K. In all three cases, which were all cw ENDOR investigations, there was no evidence reported for the presence of the large β-H hfc of 14.9 assigned to position 18. Mino et al. (*45*) have recently studied PS II using pulsed ENDOR. In that paper the radical was not specified but was suggested to be $Car^{\bullet+}$ and/or $Chl_Z^{\bullet+}$. Compared to our data the spectrum looks predominantly like $Car^{\bullet+}$ with a mixture of some $Chl_Z^{\bullet+}$ as the sample was illuminated at 77 K.

By comparison with the model system, it is clear that the β-H's from $Chl_Z^{\bullet+}$ at positions 17 and 18 appear distinct and resolved in PS II in contrast to the in vitro Chl $a^{\bullet+}$. This suggests that the protein is holding the molecule via its long side chain in a distinct conformation. MO calculations performed on the in vitro BChl *a* cation using the RHF-INDO/SP method (*30*) indicate that the magnitude of these hfc's is correlated with a distinct change in molecule conformation induced by the long side chain that involves a twist of ring D, where the β-H's 17 and 18 are bound, with respect to the rest of the tetrapyrrole system. The current ENDOR spectra indicate that the PS II protein binds Chl_Z in a distinct conformation. This fixed conformation of $Chl_Z^{\bullet+}$, relative to the in vitro Chl $a^{\bullet+}$, is probably imposed by the protein and may be of importance for its functional role.

The redox behavior of Car and its apparent function are very different from the behavior of Car in the bacterial reaction center where it acts as a quencher of the bacteriochlorophyll triplet generated by radical pair recombination. In PS II no such chlorophyll triplet quenching has been observed, and the carotenoid is thought to act instead as a redox cofactor. It appears to act as a direct electron donor to P_{680}^+ and is reduced by the Chl_Z. The interconversion of the ^{1}H ENDOR spectrum characteristic of a $Car^{\bullet+}$ to one characteristic of $Chl_Z^{\bullet+}$ reported here confirms this. The absence of ^{14}N hfc's after low-temperature illumination is clear evidence that no $Chl_Z^{\bullet+}$ is formed at low temperature, and the appearance of such couplings upon raising the temperature is also a clear indication of the interconversion. The postulated delocalization of the electron spin along the length of the carotenoid chain is consistent with the idea (*8*; see also ref *46*) that the carotenoid acts as an electronic wire, allowing electron transfer between cofactors that are rather distant from each other.

ACKNOWLEDGMENT

We gratefully acknowledge the generous permission of Prof. Dr. Thomas Prisner (Universität Frankfurt) to use the pulsed ENDOR spectrometer in his laboratory. We thank Dr. Fahmi Himo (Stockholm University) for the preliminary DFT data on the carotene cation and Drs. Friedhelm Lendzian (TU Berlin) and Sun Un (CEA Saclay) for useful discussions.

REFERENCES

1. Diner, B. A., and Babcock, G. T. (1996) in *Oxygenic photosynthesis: the light reactions* (Ort, D. R., and Yocum, C. F., Eds.) pp 213−247, Kluwer Academic Press, Dordrecht.
2. Debus, R. (1992) *Biochim. Biophys. Acta 1102*, 269−352.
3. Knaff, D. B., and Arnon, D. I. (1969) *Proc. Natl. Acad. Sci. U.S.A. 63*, 963−969.
4. Visser, J. W. M., Rijgersberg, C. P., and Gast, P. (1977) *Biochim. Biophys. Acta 460*, 36.
5. Velthuys, B. R. (1981) *FEBS Lett. 126*, 272−276.
6. Schenck, C. C., Diner, B. A., Mathis, P., and Satoh, K. (1982) *Biochim. Biophys. Acta 680*, 216−227.
7. Stewart, D. H., and Brudvig, G. W. (1998) *Biochim. Biophys. Acta 1367*, 63−87.
8. Hanley, J., Deligiannakis, Y., Pascal, A., Faller, P., and Rutherford, A. W. (1999) *Biochemistry 38*, 8189−8195.
9. Noguchi, T., Mitsuka, T., and Inoue, Y. (1994) *FEBS Lett. 356*, 179−182.
10. Pascal, A., Telfer, A., Barber, J., and Robert, B. (1999) *FEBS Lett. 453*, 11−14.
11. Deligiannakis, Y., Hanley, J., and Rutherford, A. W. (2000) *J. Am. Chem. Soc. 122*, 400.
12. Vrettos, J. S., Stewart, D. H., Cua, A., De Paula, J. C., and Brudvig, G. W. (1999) *J. Phys. Chem. B 103*, 6403−6406.
13. Konovalova, T. A., Krzystek, J., Bratt, P. J., van Tol, J., Brunel, L.-C., and Kispert, L. D. (1999) *J. Phys. Chem. B 103*, 5782−5786.
14. Faller, P., Rutherford, A. W., and Un, S. (2000) *J. Phys. Chem. B 104*, 10960−10963.
15. MacMillan, F., Rohrer, M., Krzystek, J., Brunel, L.-C., and Rutherford, A. W. (1998) in *Photosynthesis: Mechanisms and Effects* (Garab, G., Ed.) Vol. 1, pp 715−718, Kluwer Academic Press, Dordrecht.
16. Dikanov, S. A., and Tsvetkov, Yu. D. (1992) *Electron Spin−Echo Envelope Modulation (ESEEM) Spectroscopy*, pp 334−357, CRC Press, Boca Raton, FL.

17. Kurreck, H., Kirste, B., and Lubitz, W. (1988) in *Methods in Stereochemical Analysis* (Marchand, A. P., Ed.) VCH Publishers, Deerfield Beach, FL.
18. Lubitz, W., and Lendzian, F. (1996) in *Biophysical Techniques in Photosynthesis* (Amesz, J., and Hoff, A. J., Eds.) pp 255−275, Kluwer Academic Press, Dordrecht.
19. Piekara-Sady, L., Khaled, M. M., Bradford, E., Kispert, L. D., and Plato, M. (1991) *Chem. Phys. Lett. 186*, 143−148.
20. Wu, Y., Piekara-Sady, L., and Kispert, L. D. (1991) *Chem. Phys. Lett. 180*, 573−577.
21. Jeevarajan, A. S., Kispert, L. D., and Piekara-Sady, L. (1993) *Chem. Phys. Lett. 209*, 269.
22. Piekara-Sady, L., Jeevarajan, A. S., and Kispert, L. D. (1993) *Chem. Phys. Lett. 207*, 173.
23. Piekara-Sady, L., Jeevaranjan, A. S., Kispert, L. D., Bradford, E. G., and Plato, M. (1995) *J. Chem. Soc., Faraday Trans. 91*, 2881−2884.
24. Scheer, H., Katz, J. J., and Norris, J. R. (1977) *J. Am. Chem. Soc. 99*, 1372−1381.
25. Davis, M. S., Forman, A., and Fajer, J. (1979) *Proc. Natl. Acad. Sci. U.S.A. 76*, 4170−4174.
26. O'Malley, P. J., and Babcock, G. T. (1984) *Proc. Natl. Acad. Sci. U.S.A. 81*, 1098−1101.
27. Huber, M., Lendzian, F., Lubitz, W., Tränkle, E., Möbius, K., and Wasielewski, M. R. (1986) *Chem. Phys. Lett. 132*, 467−473.
28. Tränkle, E., and Lendzian, F. (1989) *J. Magn. Reson. 84*, 537−547.
29. Lubitz, W. (1991) in *Chlorophylls* (Scheer, H., Ed.) pp 903−944, CRC Press, Boca Raton, FL.
30. Käss, H., Rautter, J., Zweygart, W., Struck, A., Scheer, H., and Lubitz, W. (1994) *J. Phys. Chem. 98*, 354−363.
31. Käss, H., Lubitz, W., Hartwig, G., Scheer, H., Noy, D., and Scherz, A. (1998) *Spectrochim. Acta A 54*, 1141−1156.
32. Forman, A., Renner, M. W., Fujita, E., Barkigia, K. M., Evans, M. C. W., Smith, K. M., and Fajer, J. (1989) *Isr. J. Chem. 29*, 57−64.
33. Fajer, J. (2000) *J. Porphyrins Phthalocyanines 4*, 382−385.
34. Berthold, D. A., Babcock, G. T., and Yocum, C. F. (1981) *FEBS Lett. 134*, 231.
35. Ford, R. C., and Evans, M. C. W. (1983) *FEBS Lett. 160*, 159.
36. Davies, E. R. (1974) *Phys. Lett. 47A*, 1−2.
37. Atherton, N. M. (1993) *Principles of Electron Spin Resonance*, Ellis Horwood Limited, Chichester.
38. Rohrer, M., Plato, M., MacMillan, F., Grishin, Y., Lubitz, W., and Möbius, K. (1995) *J. Magn Reson., Ser. A 116*, 59−66.
39. Kurreck, H., Bock, M., Bretz, N., Elsner, M., Kraus, H., Lubitz, W., Müller, F., Geissler, J., and Kroneck, P. M. H. (1984) *J. Am. Chem. Soc. 106*, 737.
40. Rigby, S. E. J., Nugent, J. H. A., and O'Malley, P. J. (1994) *Biochemistry 33*, 10043.
41. Jegerschöld, C., MacMillan, F., Lubitz, W., and Rutherford, A. W. (1999) *Biochemistry 38*, 12439−12445.
42. Käss, H., Bittersmann-Weidlich, E., Andréasson, L.-E., Bönigk, B., and Lubitz, W. (1994) *Chem. Phys. 194*, 419−432.
43. Käss, H. (1995) Ph.D. Dissertation, Technische Universität Berlin, Germany.
44. MacMillan, F., Lendzian, F., Renger G., and Lubitz, W. (1995) *Biochemistry 34*, 8144−8156.
45. Mino, H., Kawamori, A., and Ono, T.-A. (2000) *Biochim. Biophys. Acta 1457*, 157−165.
46. Gruszecki, W. I., Strzalka, K., Radunz, A., Kruk, J., and Schmid, G. H. (1995) *Z. Naturforsch. 50C*, 61−68.

BI002029L